Journal of Innovative Optical Health Sciences
Vol. 2, No. 2 (2009) 131–135

World Scientific
www.worldscientific.com

MONTE CARLO SIMULATION OF POLARIZED LIGHT SCATTERING IN TISSUES

TIANLIANG YUN*, WEI LI, XIAOYU JIANG and HUI MA
Laboratory of Optical Imaging and Sensing
Graduate School at Shenzhen, Tsinghua University
Shenzhen 518055, China
Key Laboratory for Molecular and
Nanosciences of Education Ministry
Department of Physics, Tsinghua University
Beijing 100084, China
**ytl05@mails.tsinghua.edu.cn*

We investigate the propagation of polarized light in fibrous tissues such as muscle and skin. The myofibrils and collagen fibers are approximated as long cylinders and the tissue phantom is composed of spherical and cylindrical structures. We apply Monte Carlo method based on this phantom to simulate and analyze polarization imaging process of muscle. The good agreement between the simulation results and the experimental results validate the assumption of the phantom composition. This paper also presents how to describe the fiber orientation distribution and tissue anisotropy according to three parameters derived from the polarization imaging.

Keywords: Monte Carlo; polarized light; anisotropy; cylindrical scatterer.

1. Introduction

The biological tissues are highly-scattering media, so the background noise arising from diffusive photons has a great impact on most of biophotonics imaging technologies. Polarization imaging plays an important role in eliminating the background noise by selecting photons backscattered from the superficial layers. However, there has not been an effective theory to describe polarized light propagating in the tissues.

In 1995, the source code of Monte Carlo program of photon transport in multilayered tissues was published,[1] in which the scatterers were regarded as spheres. Since then, Monte Carlo simulation has increasingly become an important and useful method in investigating the propagation of photons in turbid medium, and many research papers in this field have been reported. Some recent research in Monte Carlo simulation focuses on the polarization characteristic of photons.[2,3] However, the sphere assumption is not valid for all scatters when considering the real structure of tissues related with the polarization effect, for example, myofibrils in muscle are approximate cylinders. The scattering properties of cylindrical particles has been reported by several researchers.[4,5] In this paper, we present a tissue phantom composed of spherical and cylindrical particles and the simulation results and analysis show its feasibility in studying the propagation of polarized light in turbid medium.

2. Monte Carlo Simulation Method

We complete the Monte Carlo program based on our previous version that simulated the polarized light propagation in the isotropic medium composed of spherical scatterers. The program starts with launching millions of photons, then tracks and records the photon one by one, until all the photons are absorbed or escape from the medium. Before tracking the photon, we calculate a series of scattering matrices of spherical and cylindrical scatters respectively, which depend on the size parameter, the complex index of refraction of the particle, as well as the incident and scattered angle of the photon. According to an analytical solution of the Maxwell equations,[6] we obtain the phase function of an infinitely long cylindrical scatter at oblique incidence. The calculations show that the light scattered by an infinitely long cylinder at an angle ξ is a conical wave, with the cylinder as the axis of the cone having a half angle ξ [see Fig. 1]. The scattering intensity around the cone for a certain ξ depends on the scattering direction defined by θ. Thus, the phase function of infinitely long cylinder, which is related to both ξ and θ, can be calculated from the corresponding scattering matrices $M(\xi, \theta)$ [see Fig. 2]. Then the direction of propagation on the cone is determined according to the phase function. In Fig. 2, the calculations are performed for the cylinder having a radius of $1\,\mu$m, a refractive index inside and outside the cylinder of 1.4 and 1.35 respectively. It shows that with the angle ξ increasing, light tends to propagate in the incident direction ($\theta = 0$).

The initial feature of photons, including location, direction of propagation, and polarization state defined by the Stokes vector $S = [I, Q, U, V]$,

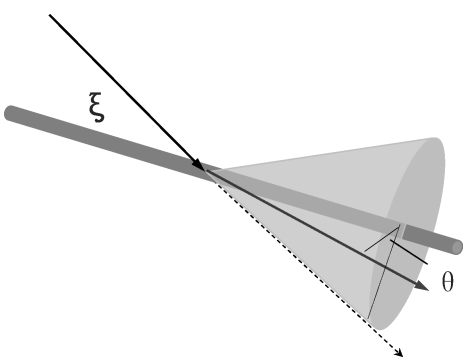

Fig. 1. Scheme of light-scattering characteristics by an infinitely long cylinder.

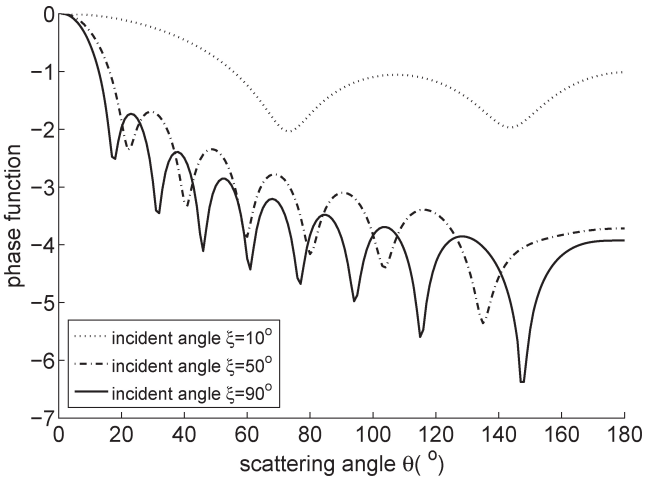

Fig. 2. Scattering phase functions of an infinitely long cylinder for different incident angles ξ.

are determined by given conditions. The photon is moved a propagation distance Δs that is calculated according to the total scattering coefficient, the absorption coefficient of the media, and the random number. Then, according to the direction of propagation, we can determine the next scattering location of the photon. The type of scatterer hit by photon depends on the proportion of scattering coefficients corresponding to different scatterers. The scattering coefficient of cylinders is related to the incident angle ξ.[7]

$$\mu_s(\xi) = Q_{\text{sca}}(\xi) \cdot d \cdot C_A, \tag{1}$$

where Q_{sca} is the scattering efficiency, d is the diameter of cylinder, and C_A is the density of the cylinders. The $\mu_{s,\text{cyl}}$ mentioned below is a given value when $\xi = 90^\circ$ ($\mu_{s,\text{cyl}} = \mu_{s,\text{cyl}(\xi=90^\circ)}$), and other values of $\mu_s(\xi)$ can be calculated for the given function of Q_{sca}. The total scattering coefficient of the media is approximately the sum of scattering coefficient of two types of scatters ($\mu_{s,\text{total}} = \mu_{s,\text{sph}} + \mu_{s,\text{cyl}}$). Additionally, the arrangement of the cylindrical scatters in real tissues is not exactly parallel but a Gaussian distribution along a direction, which is described with FWHM $\Delta\eta$ in simulations.

When the type of scatterer is determined, in addition to the incident and the scattering direction obtained from the phase function, the corresponding scattering matrix is selected and then $S' = M \times S$ is calculated. Repeat the steps above for a photon, until its life ends when it passes through a boundary or when its weight W value falls below a threshold (0.01).

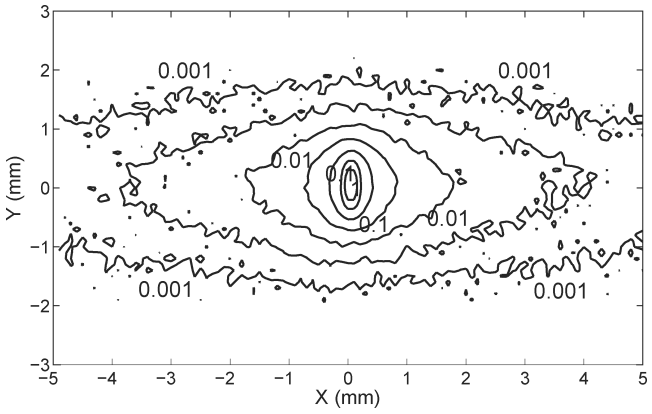

Fig. 3. $R(x, y)$ pattern obtained from Monte Carlo simulations of a semi-infinite turbid medium containing cylinders along the axis with $\Delta\eta = 15^\circ$.

3. Validation of the Monte Carlo Simulation Program

In this section, we concentrate on the part of program when the tissue phantom contains cylindrical scatterers only ($\mu_{s,\mathrm{sph}} = 0$). We did some simulations and compared the results to those that had been published.

Figure 3 shows the spatially resolved reflectance $R(x, y)$ obtained from the Monte Carlo simulation of a medium that contains cylinders only with $r = 1\,\mu$m, $\Delta\eta = 15^\circ$ along x axes, $\mu_{s,\mathrm{cyl}} = 300\,\mathrm{mm}^{-1}$. The main axes of the intensity contour ellipses are perpendicular to the cylinders of the tissue at small distances (< 1 mm) but parallel to the cylinders at large distances (> 1 mm). The similar result was published in 2004,[4] so this simulation result confirms the confidence of our Monte Carlo program.

4. The Monte Carlo Simulation of Polarization Imaging

We apply the program to simulate the experiment of polarization imaging. The experiment setup is illustrated in Fig. 4.[8]

In the experiment, the muscle tissues were laid on X–Y plane and the myofibrils of that were aligned parallel to X axis. The collimated 650-nm light from a $1W$ LED passed through a linear polarizer P1 and then illuminated the sample at an angle of 20° to the normal direction of the sample surface. Backscattered photons from the sample were focused after passing through a linear polarizer P2 and recorder by a CCD. We acquired a series of images $I(\theta_i, \theta_s)$ corresponding to different

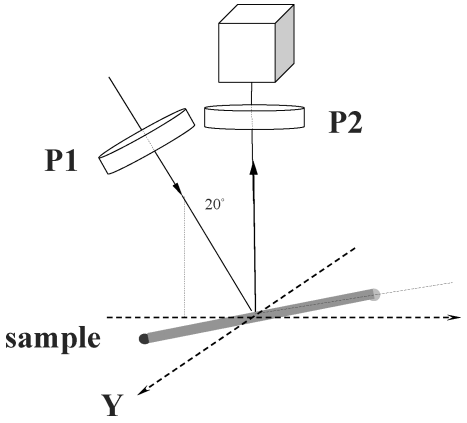

Fig. 4. Scheme of experimental setup.

combinations of θ_i and θ_s (θ_i and θ_s represent the incident and detection polarization angles) by rotating P1 and P2 separately. Linear Differential Polarization (LDP) was calculated as the detected intensity difference with two orthogonal polarization analyzers, respectively.[8]

$$LDP(\theta_i, \theta_s) = I(\theta_i, \theta_s) - I(\theta_i, \theta_s + \pi/2). \qquad (2)$$

We plot the normalized LDP $(\theta_i, 0)$ as functions of θ_i, that is a cosine curve as shown in Fig. 5.

In the simulation, we studied two tissue-phantoms of muscle respectively: (1) spherical scatterers only, and (2) spherical and cylindrical scatterers. For the phantom (1), the minimum of LDP equals to -1 in the case of normally incident light, and less than -1 in the case of inclined incident light, which do not agree with the experimental results. But for the phantom (2), the simulation results can match experiment well by varying the proportion of the two scatterers (20% spheres, 80% cylinders), as shown in Fig. 5.

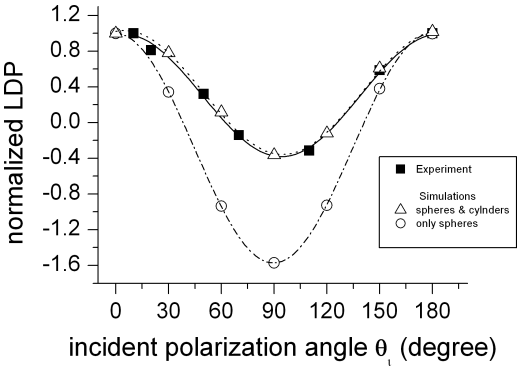

Fig. 5. Dependence of Linear Differential Polarization on incident polarization angle.

According to a great mount of data from simulations and experiments, we find that LDP can be expressed as[8]:

$$LDP(\theta_i, \theta_s) = \sqrt{A\cos(4\theta_s - \varphi_1) + B}\cos(2\theta_i - \varphi_2(\theta_s)) + C\cos(2\theta_s - \varphi_3). \quad (3)$$

In the experiment, the fibers were aligned at a preset angle, and then the LDP(θ_i, θ_s) data series at every pixel of image could be obtained. We can obtain the experimental value of parameter A, B, C, φ_1 and φ_3 by curve fitting according to Eq. (3), and the similar processing is completed in simulation to get the above parameters. The results imply that $\varphi_3/2$ can indicate the orientation angle of cylindrical component in tissue, as shown in Fig. 6.

In Fig. 7, the distribution of the orientation of fibers ($\varphi_3/2$) at all pixels of the sample shows that the fibers in tissue have a Gaussian distribution, which validate the assumption in simulation.

In addition, we find that A/B derived from Eq. (3) is unaffected by sample orientation and also insensitive to tissue clearing. We think that A/B may be related to the structural anisotropy of the sample. The comparison of experimental results for different biological tissues is shown in Table 1.

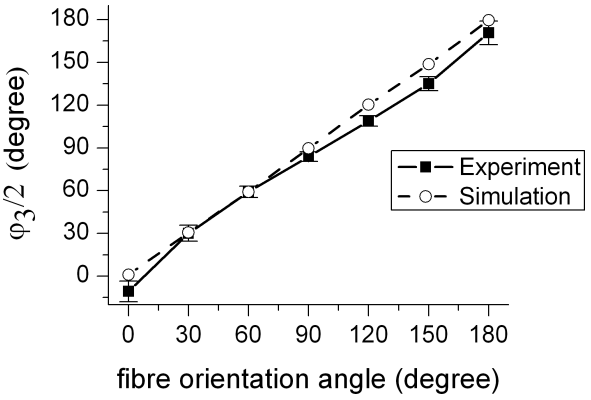

Fig. 6. Dependence of $\varphi_3/2$ on orientation of the cylindrical scatterers.

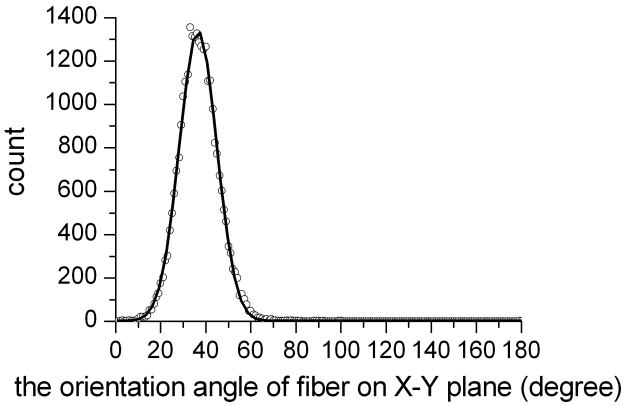

Fig. 7. Distribution of the orientation of fibers in a 1.76 mm × 1.76 mm area of sample.

In Table 1, we can see that for the sample with prominent fibrous structures like porcine skeleton muscle, the value of A/B is larger than that of known isotropic tissue like porcine liver. Compared with samples in group 1 and 3, those in group 2 and 4 have smaller A/B due to the irregular alignment of the fibers, which reduces the structural anisotropy.

To validate the assumption about A/B, we apply the Monte Carlo simulation with tissue phantom composed of spherical and infinitely long cylindrical scatters. Similarly, A/B is unaffected by the cylinders' orientation but is sensitive to the ratio of scattering coefficients of two types of scatterers and the width of the Gaussian distribution of fibers. With increasing proportion of spherical scatterers or the width $\Delta\eta$ of the Gaussian distribution, the tissue phantom becomes less anisotropic and A/B decreases, as shown in Fig. 8. Therefore, the simulation method validates the experimental results and the idea that the variation of A/B can quantitatively figure out the anisotropy of fibrous structure.

Table 1. Comparison of different samples.

Group	Sample	A/B (Average ± RSD)
1	Porcine skeleton muscle with regular alignment of fibers parallel to sample surface	0.95 ± 7.4%
2	Porcine skeleton muscle with irregular alignment of fibers parallel to sample surface	0.63 ± 33%
3	Gallinaceous skeleton muscle with regular alignment of fibers parallel to sample surface	0.96 ± 4.2%
4	Gallinaceous skeleton muscle with irregular alignment of fibers parallel to sample surface	0.65 ± 38%
5	Porcine fatty tissue	0.17 ± 53%
6	Porcine liver	0.07 ± 57%

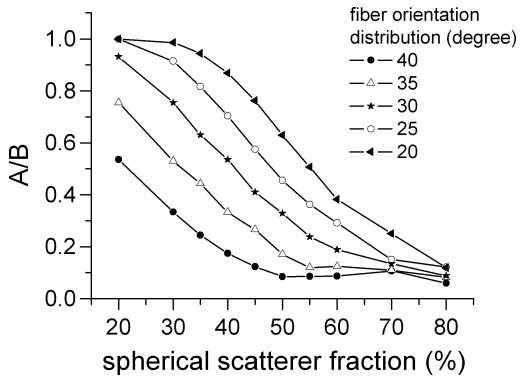

Fig. 8. Dependence of A/B on the fraction of spherical scatterers and the width of the Gaussian distribution.

5. Conclusion

In summary, we present and validate the model composed of spherical and infinitely long cylindrical scatters describing the fibrous tissues. We apply Monte Carlo simulation based on this model to simulate and explain quantitatively the experimental results in polarization imaging of fibrous tissues such as muscle and skin. This tissue phantom is suitable to approach the real sample by varying several parameters, such as the orientation distribution of the cylindrical scatters, the proportion, and the radius of the two scatters. The correlation between the Monte Carlo simulation and experimental results of muscle shows that the model can be used to reveal structural characteristics of tissues qualitatively and even quantitatively from two aspects: (1) The orientation of cylindrical structure in tissues can be calculated by fitting backscattering polarization difference when varying incident polarized angles, and the experimental data processing demonstrates that the fibers are arranged along one direction and have a Gaussian distribution; (2) We find that the value of A/B is related to the proportion of the cylindrical scatters and the width of orientation distribution, so that the variable in the model, A/B, can be an indicator of anisotropy of fibrous tissues. We believe that some pathologic information about skin or muscle, correlating with fiber orientation distribution and the amount of fibers,[9] can be figured out by measuring the variation of A/B. These above findings show exciting potentials of this anisotropic model and polarization imaging parameters for therapeutic and diagnostic applications.

Acknowledgment

This work was supported by National Natural Science Foundation of China (Grant 60578003), and Ministry of Science and Technology (Grant 2006CB70570), China.

References

1. Wang, L. V., Jacques, S. L. and Zheng, L., *Comput. Meth. Prog. Biomed.* **47**, 131 (1995).
2. Ramella-Roman, J., Prahl, S. and Jacques, S. L., *Opt. Express* **13**, 4420 (2005).
3. Ramella-Roman, J., Prahl, S. and Jacques, S. L., *Opt. Express* **13**, 10392 (2005).
4. Kienle, A., Forster, F. and Hibst, R., *Opt. Express* **29**, 2617 (2004).
5. Kienle, A. and Hibst, R., *Phys. Rev. Lett.* **97** (2006).
6. Bohren, C. F. and Hurman, D. R., *Absorption and Scattering of Light by Small Particles* (John Wiley and Sons, New York, 1983).
7. Kienle, A. and Wetzel, C., *J. Biomed. Opt.* **12** (2007).
8. Jiang, X.-Y., Zeng, N., He, Y.-H. and Ma, H., *Progress in Biochemistry and Biophysics* **34**, 659 (2007).
9. Ranasinghesagara, J. and Yao, G., *Opt. Express* **15**, 3998 (2007).